Well-defined mesoporosity on lignocellulosic-derived activated carbons

Ana Silvestre-Albero[1], *Maraisa Gonçalves*[1], *Tsutomu Itoh*[2], *Katsumi Kaneko*[2], *Morinobu Endo*[2], *Matthias Thommes*[3], *Francisco Rodríguez-Reinoso*[1] *and Joaquin Silvestre-Albero*[1,*]

[1] Laboratorio de Materiales Avanzados, Departamento de Química Inorgánica-Instituto Universitario de Materiales, Universidad de Alicante, Ap. 99, E-03080 Alicante (Spain), [2] Exotic Nanocarbon Research Center, Shinshu University, 4-17-1 Wakasato, 380-8553 Nagano (Japan), [3] Quantachrome Instruments, 1900 Corporate Drive, Boynton Beach, FL33426 (USA)

ABSTRACT: Activated carbons with a highly developed mesoscale cavitation-linked structure have been prepared from natural products (e.g. peach stones) by combining chemical and physical activation processes. Characterization results show that these materials exhibit a large "apparent" surface area (~ 1500 m^2/g) together with a well-defined mesoporous structure, i.e. large cavities connected to the external surface through narrower mesoporous necks (cavitation effects).

[1] *Corresponding author. Tel/Fax: +34 96590 9350/+34 96590 3454. E-mail address: joaquin.silvestre@ua.es (J. Silvestre-Albero)

1. Introduction

Activated carbons have been widely used in the traditional research fields of adsorption, gas separation, catalysis, gas/energy storage, and so on, due to their tunable textural properties in terms of surface area and pore volume [1]. Unfortunately, although activated carbons prepared using the conventional physical (CO_2 or H_2O) and chemical activation (KOH or H_3PO_4) procedures exhibit a well-developed porous structure, this is mainly located in the microporous range with a relatively small development of mesoporosity. Actual demands in research fields dealing with large molecules (e.g. drug delivery, biomedical application, purification of biofluids, water purification technologies) require the design of new porous carbons with extended pore diameter in the mesoporous range (pore dimensions above 2 nm) [2-4]. Mesopores constitute the pathways for large molecules to access the inner porous structure (primary adsorption sites), thus improving the adsorption kinetics.

Nowadays, activated carbons with a highly developed mesoporous structure are prepared using either hard or soft template technology [5]. The first synthesis of an ordered mesoporous activated carbon was reported by Ryoo et al. in 1999 using nanocasting technology [6]. Infiltration of sucrose inside the mesoporous channels of the MCM-48, followed by carbonization and the subsequent removal of the silica framework gave rise to hexagonally ordered carbon nanorods (CMK-1). Similar ordered mesoporous carbon materials were prepared using other porous silica scaffolds such as MCM41 and SBA15, and also a colloidal silica template [7, 8]. Alternative methods for the synthesis of mesoporous carbon via self-assembly (soft template technology) using a block copolymer as a template and a resin as a carbon precursor have been recently reported in the literature [9, 10]. Unfortunately, both hard and soft template technologies exhibit important drawbacks, mainly associated with the cost of the copolymer scaffold and, the additional synthesis and sacrificial use of the ordered mesoporous scaffold, in the hard template technology.

Natural products based in lignocellulosic residues (olive stones, peach stones, and so on) are nowadays the most appropriate candidates for cost effective preparation of activated carbons. Due to the presence of a well-defined inherent macroporous structure (inner cellular channels), natural products have been

traditionally though as promising candidates for the development of mesoporosity. However, as described above the conventional physical and chemical activation procedures have always provided materials with a well-developed porous structure but almost restricted to the microporous range [11, 12]. Recent studies described in the literature have anticipated that incorporation of inorganic species ($ZnCl_2$ or $CaCl_2$) into the carbon precursor (coconut shell and olive stones) can modify the carbon gasification reaction and, consequently, the porous structure development [13, 14]. N_2 adsorption measurements on these samples have shown the presence of a highly developed microporous structure, i.e. a large nitrogen adsorption capacity at low relative pressures ($p/p_0 < 0.1$), together with an increased adsorption capacity at high relative pressures (above $p/p_0 \sim 0.6$), which can be attributed either to condensation in the interparticle space or, more probably, to the presence of ill-defined mesoporosity.

With this in mind, in this manuscript we show that the appropriate combination of chemical activation with $ZnCl_2$ followed by physical activation with CO_2 and catalyzed by $CaCl_2$ permits the preparation of activated carbons with a highly developed well-defined mesoporosity starting from a lignocellulosic precursor. To our knowledge, this is the first time that well-defined mesoscale cavitation-linked activated carbons are prepared starting from natural products. The analysis of nitrogen and argon adsorption isotherms suggests that the mesoporous structure of the synthesized materials is constituted by large mesoporous cavities connected with the external surface through narrower mesoporous necks, i.e. cavitation effects are clearly observed. The manuscript will be devoted to activated carbons prepared from peach stones as a raw material, although the experimental details and results can be extended to other lignocellulosic residues (e.g. olive stones or coconut shells).

2. Experimental

2.1 *Sample preparation*. Mesoporous activated carbons were prepared from peach and olive stones combining two different activation treatments. First a chemical activation treatment with $ZnCl_2$ was performed followed by a catalyzed physical activation using CO_2 as activating agent and $CaCl_2$ as catalyst. Briefly, the lignocellulosic precursor (particle size 2.0-2.8 nm) was impregnated with an

aqueous solution of $ZnCl_2$ (1.5 g of precursor for 1 ml of solution) at 358 K for 7h. The impregnated sample was submitted to a thermal treatment under a N_2 atmosphere up to 973 K for 2 h. After cooling down, the carbonized sample was washed with HCl acid (10%) and distilled H_2O until complete removal of $ZnCl_2$ (sample LMA21). In a subsequent step, sample LMA21 (obtained from peach stones) was impregnated with an aqueous solution of $CaCl_2$ (4.5 wt.% Ca) at 358 K for 7h. The dried sample was submitted to a thermal treatment at 1123 K for 2h under a CO_2 atmosphere. After cooling down, the activated sample (LMA22) was washed with hot HCl (10%) acid in order to remove the catalyst followed by distilled water until a pH ~ 7.

2.2 *Sample characterization.* Textural properties of the synthesized materials were evaluated by high-resolution N_2, CO_2 and Ar adsorption/desorption isotherms at 77.4 K, 273 K and 87.3 K, respectively. Adsorption experiments were performed at the University of Alicante in a home-made manometric equipment and at Quantachrome Instruments, using an Autosorb1-MP. Further analysis of the microporous structure was performed by N_2 adsorption measurements after n-nonane pre-adsorption together with immersion calorimetry measurements into liquids of different molecular dimensions [15]. Pre-adsorption of n-nonane was performed in the manometric equipment described before using the following procedure: after degassing at 523 K for 4h, the sample was exposed to n-nonane (Aldrich, 99%) for 30 min at 77 K and then left in contact with the liquid for 3h at room temperature. After the pre-adsorption, the sample was degassed at 298 K overnight prior to the second measurement of the N_2 adsorption isotherm at 77 K. Immersion calorimetry measurements were performed in a C80D calorimeter at 303 K. Prior to the experiment, the sample was degassed under vacuum at 523 K for 4h in a glass bulb. After sealing the bulb in vacuum, the sample ampoule was introduced into the calorimetric chamber containing the immersion liquid. Once thermal equilibrium was reached, the brittle end of the ampoule was broken and the heat released was followed with time.

TEM analysis was performed by use of high resolution transmission electron microscopy (HR-TEM; JEOL Ltd., JEM-2100F).

3. Results and discussion

3.1 *Nitrogen adsorption isotherms at 77.4 K before and after n-nonane pre-adsorption*

Nitrogen adsorption-desorption isotherm at 77.4 K for the chemically activated carbon LMA21 exhibits a type I, according to the IUPAC classification, corresponding to a pure microporous material (see Figure 1a). Furthermore, the presence of a broad knee at low relative pressures suggests the presence of a broad pore size distribution, i.e. presence of narrow and wide micropores. This assumption can be clearly discerned after application of the non-local density functional theory (NLDFT) method to the nitrogen data assuming a slit-shape pore geometry [16, 17]. The pore size distribution for sample LMA21 (not shown) exhibits a broad peak centered at ca. 1 nm together with a shoulder between 1.5 nm and 3.0 nm, due to the presence of wide micropores and a certain proportion of small mesopores. This result is in close agreement with previous studies described in the literature for chemically activated carbons prepared using $ZnCl_2$ [12, 18, 19]. The "apparent" surface area of the synthesized material is as high as 1425 m^2/g, with a total pore volume of 0.70 cm^3/g at a relative pressure of 0.99 (see Table 1).

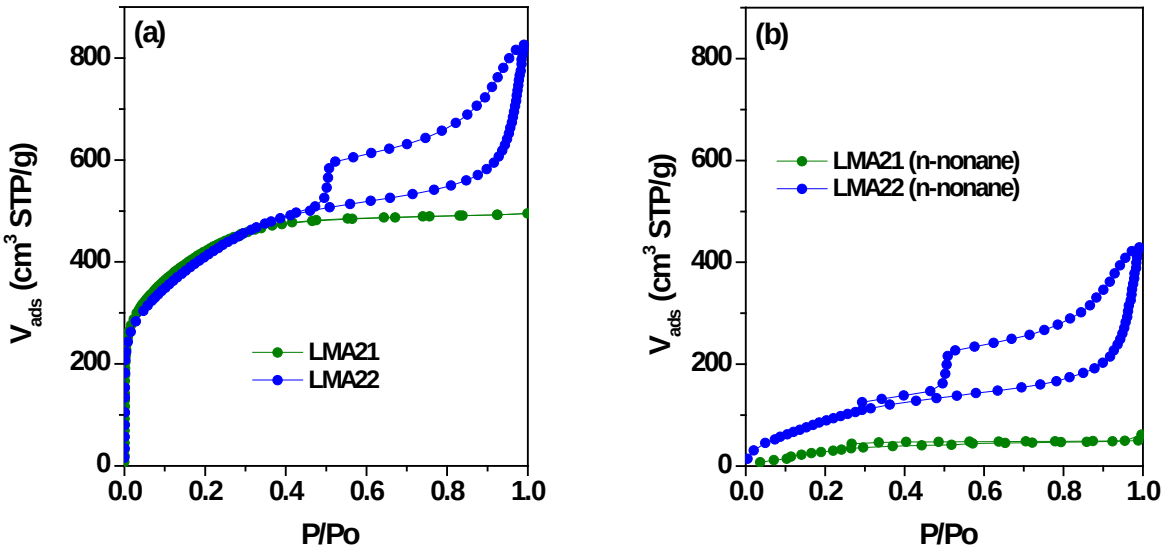

Figure 1. N_2 adsorption/desorption isotherms at 77.4 K for the synthesized materials before and after n-nonane pre-adsorption.

A completely different scenario occurs for the same sample after a subsequent physical activation with CO_2 and catalyzed by $CaCl_2$. The new material (labeled LMA22) exhibits a combination of type I and type IV isotherms. Interestingly, the microstructure of the newly synthesized activated carbon remains mainly unchanged compared to the raw material, LMA21, while there is a sudden increase in the amount of nitrogen adsorbed above p/p_0 ~ 0.4, up to a total volume around 830 cm^3 STP/g. The capillary condensation is accompanied by a wide hysteresis loop indicating a delay both in the condensation and evaporation steps. Consequently, physical activation with CO_2 catalyzed by $CaCl_2$ does not produce changes in the microporous structure of the raw material while there is a drastic development of the mesoporosity. The textural parameters deduced from the nitrogen adsorption data (Table 1) provide an "apparent" surface area of 1490 m^2/g, a value very similar to the one obtained for the original carbon. As described before, the micropore volume remains mainly unaffected compared to the original sample while there is a four-fold increase in the mesopore volume (up to 0.63 cm^3/g).

Previous studies described in the literature have shown that the combination of a chemical activation treatment with $ZnCl_2$ followed by a conventional physical activation with CO_2 (in the absence of $CaCl_2$) gives rise to carbon materials with a highly developed microporous structure (up to 2000 m^2/g), although with a scarce development of mesoporosity [19]. Taking into account these premises, the results described above clearly show that $CaCl_2$ acts as a catalyst favoring the carbon gasification reaction (C-CO_2), with the subsequent formation of mesocavities.

Table 1. Textural properties for the different samples obtained from the N_2 adsorption data.

Sample	S_{BET} (m^2/g)	V_0 (cm^3/g)	V_{meso} (cm^3/g)	V_t (cm^3/g)
LMA21	1425	0.54	0.16	0.70
LMA22	1490	0.52	0.63	1.15
LMA21 (n-nonane)	170	0.00	0.08	0.08
LMA22 (n-nonane)	480	0.14	0.45	0.59

The selective blocking of the porosity using long hydrocarbons is a very useful method to get an understanding of the porous structure on porous solids. This method developed by Gregg and Langford is based on the strong adsorption that these molecules experience in the micropores, in such a way that a vacuum treatment of the saturated sample will only remove the hydrocarbon from the larger pores, i.e. mesopores and macropores [20, 21]. Figure 1b shows the nitrogen isotherms at 77.4 K for both samples (LMA21 and LMA22) after n-nonane pre-adsorption. As it can be observed, the chemically activated sample exhibits a complete blocking of the porous structure by the hydrocarbon, in accordance with its pure microporous structure. On the contrary, sample LMA22 exhibits an important depletion of the nitrogen adsorption capacity at low relative pressure, i.e. there is a drastic blocking of the microporosity, while the capillary condensation and evaporation in the mesoporous region remains unaffected. These results suggest that i) samples LMA21 and LMA22 contain a large volume of micropores and ii) in the case of the LMA22 sample these micropores are independent of the mesoporous structure, i.e. the blocking of the micropores is not affecting the mesoporous structure. More probably, micropores are located in the inner walls of the mesopores although the presence of some micropores in the external surface can not be ruled out. Textural properties after n-nonane pre-adsorption are summarized in Table 1. As described before, the microporosity is completely blocked in sample LMA21 after n-nonane pre-adsorption while on sample LMA22 the microporosity is highly affected, while the mesoporosity (mesopore volume) remains mainly unchanged.

3.2 *High-resolution transmission electron microscopy (HR-TEM)*

The morphology of the porous structure in sample LMA22 has been carefully characterized by high-resolution transmission electron microscopy. Figures 2a and 2b show the TEM images of a considerable thick region, while Figure 2c corresponds to the edge region of the carbon sample. TEM images show that the structure of activated carbon LMA22 is constituted by block units consisting of curvy carbon layers mutually linked to each other creating a three dimensional carbon frame with considerably uniform voids of several nm in width. As there are single graphene-like platelets in the block units, as

shown in Figure 2c, the interstices between the nanosized platelets should correspond to the micropores and the narrow mesopores. Therefore, the mesocavities of several nm should be connected with the micropores and narrow mesopores in the block unit. This pore model would be supported by the adsorption hysteresis data given later.

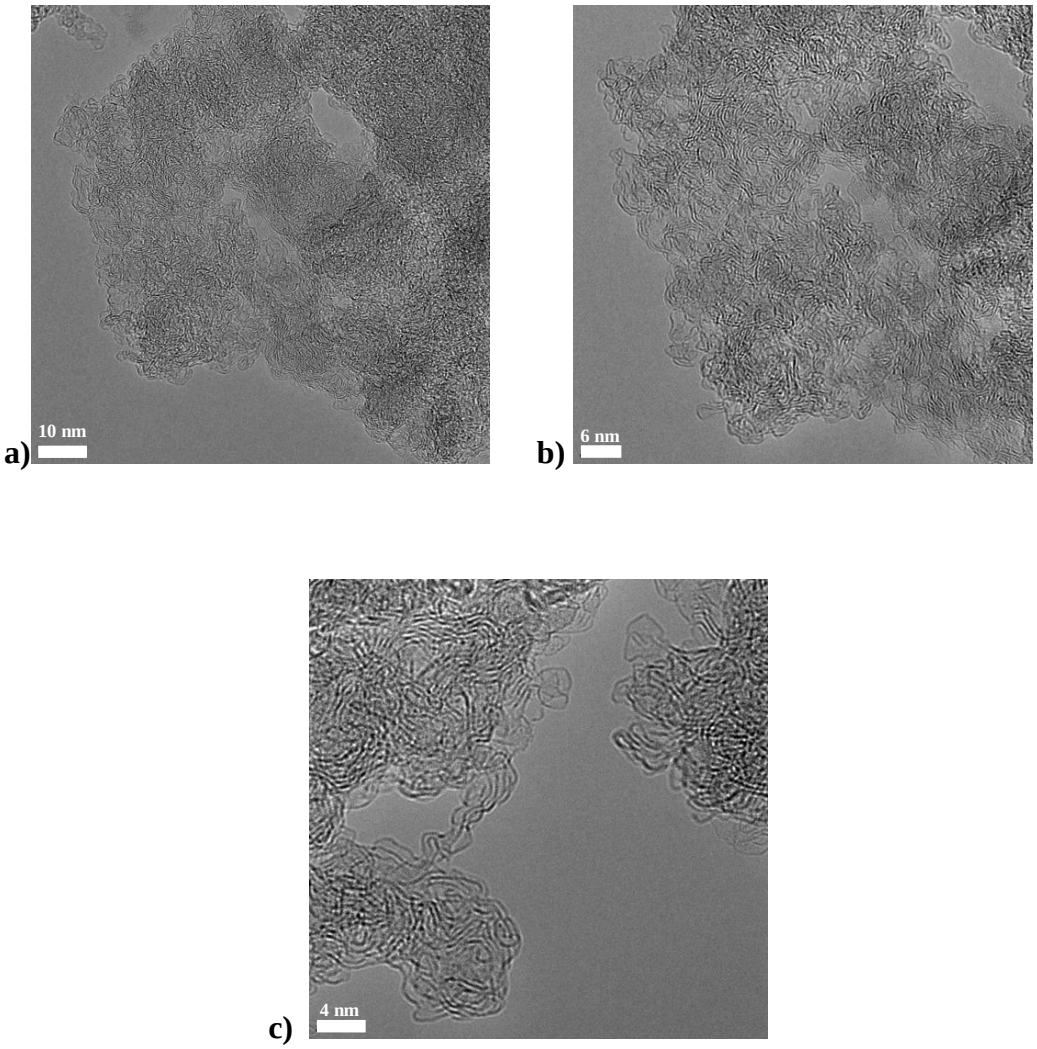

Figure 2. TEM images of activated carbon LMA22.

3.3 *Immersion calorimetry measurements at 303 K*

In a final step, the size of the micropores has been analyzed using immersion calorimetry into liquids of different molecular dimensions. In this sense, Table 2 summarizes the enthalpy of immersion ($-\Delta H_{imm}$) in J/g for dichloromethane, benzene, n-hexane, 2,2-dimethyl-butane and α-pinene. As it can be observed, even a molecule such as α-pinene, with a kinetic diameter of 0.7 nm, is able to access the inner porous structure of both sample (LMA21 and LMA22), i.e. the enthalpy of immersion is very similar compared to the one obtained with a small molecule such as dichloromethane (0.33 nm). In the absence of specific interactions at the solid-liquid interface, the enthalpy of immersion of a solid into a liquid can be used as an estimation of the total surface available for a selected liquid [15]. The results reported in Table 2 suggest that the micropores present in the chemically activated LMA21 carbon and the mesoporous LMA22 sample are all above a pore size entrance of 0.7 nm, the kinetic diameter of α-pinene, in close agreement with NLDFT data described above for sample LMA21.

Table 2. Enthalpy of immersion ($-\Delta H_{imm}$) in J/g into liquids with different molecular dimensions (dichloromethane, 0.33 nm; benzene, 0.37 nm; n-hexane, 0.43 nm; 2-methyl-pentane, 0.49 nm; 2,2-dimethyl-butane, 0.56 nm; α-pinene, 0.70 nm).

Sample	DCM	Bz	n-hx	2,2-DMB	α-pinene
LMA21	132	116	110	103	101
LMA22	130	127	128	108	118

3.4 *Nitrogen adsorption-desorption isotherms at 77.4 K and argon adsorption at 87.3 K*

Nitrogen adsorption-desorption isotherms at 77.4 K clearly show the presence of an important hysteresis phenomena of type II, according to the IUPAC classification, in sample LMA22. This type of phenomenon occurs for samples where the mesopores are connected to the external surface through narrow necks, as in the ink-bottle pores (see inset in Figure 3a). Depending on the neck diameter, the hysteresis can be attributed to the *pore blocking* or *cavitation* effect. A simple test to determine the mechanism of evaporation, and consequently, to get a clear image of the mesoporous network consist in the measurement of the adsorption-desorption isotherm for different adsorptives [22]. If pore blocking is the dominant mechanism, the evaporation will be defined by the neck diameter and will be independent of the adsorptive used. On the contrary, if cavitation is the dominant mechanism, the evaporation will proceed through spontaneous formation of bubbles inside the large mesopores and evaporation of the mesopore body by diffusion through the neck, which remains filled down to a lower relative pressure. Due to the different thermodynamic states of nitrogen and argon, the pore size distribution obtained from the desorption branches in case of cavitation, i.e. the evaporation from the pore body, must be sensitive to the nature of the adsorptive and not to the neck diameter. Thus, for a given adsorptive and temperature, the presence of one or another evaporation mechanism may depend on the neck diameter, i.e. there is a critical neck diameter (W_c) below which the evaporation mechanism changes from *pore blocking* to *cavitation*. This critical neck diameter has been established around 5-6 nm for N_2 at 77 K [22, 23].

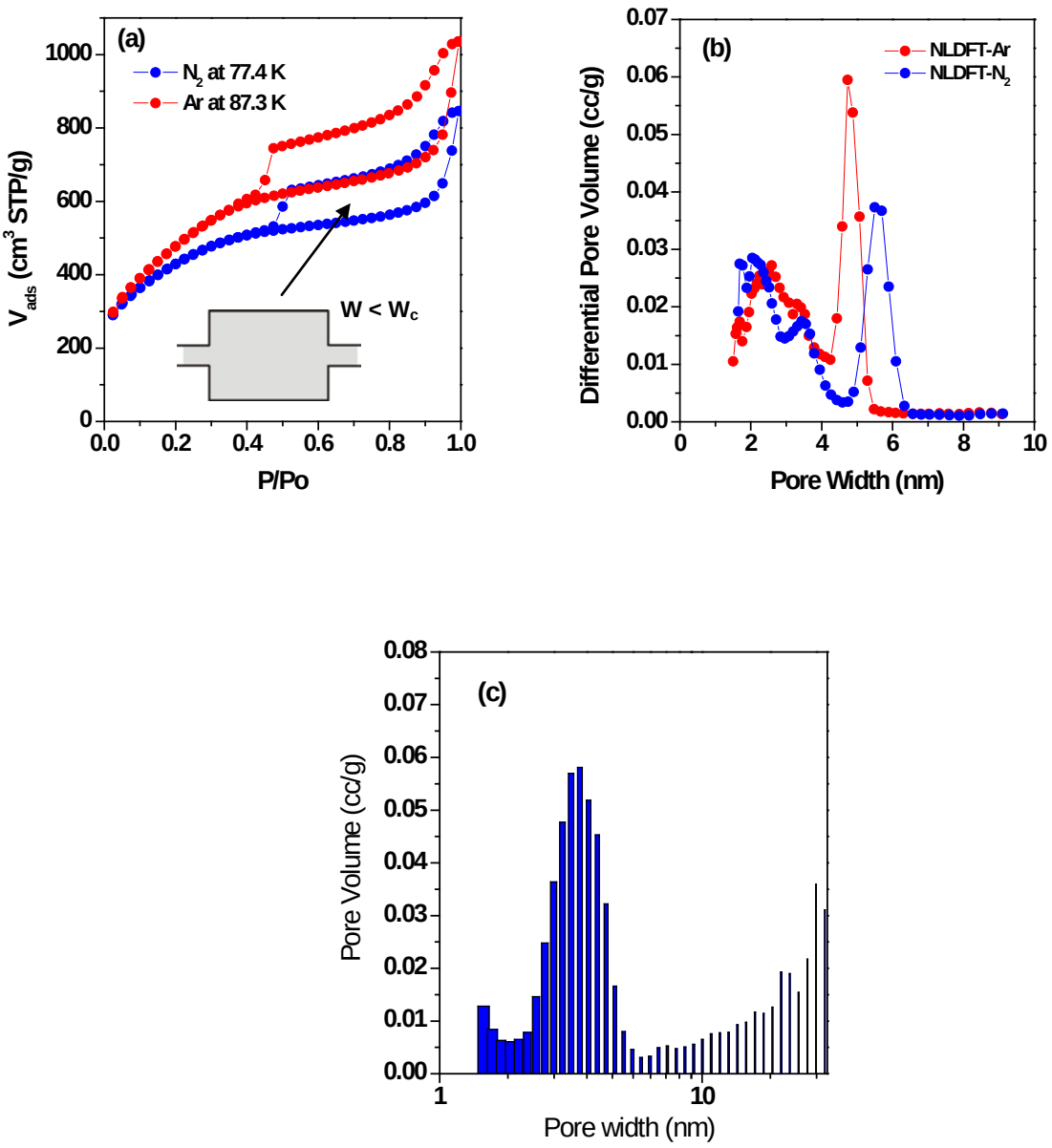

Figure 3. (a) N_2 and Ar adsorption-desorption isotherms for sample LMA22 at 77.4 K and 87.3 K, respectively, (b) pore size distribution profile after application of the NLDFT method to the nitrogen and argon desorption data (assuming a cylindrical-shape pore model) and (c) pore size distribution profile after application of the novel QSDFT method only to the adsorption branch of the N_2 isotherm (assuming slit/cylindrical-shape pore model) [24]. Inset shows a schematic representation of the large mesoporous cavities connected with the external surface through narrower micro/mesopore necks.

Figure 3a compares the nitrogen and argon adsorption-desorption isotherms for sample LMA22 at 77.4 K and 87.3 K, respectively. Interestingly, the shape of the isotherms is mainly the same independently of the adsorptive used. In both cases there is a large amount adsorbed at low relative pressures due to the filling of the micropores, together with the capillary condensation at around p/p_0 ~ 0.8-0.9. The total amount adsorbed at p/p_0 of 1 is larger for argon (V_t STP: 1040 cm^3/g) compared to nitrogen (V_t STP: 853 cm^3/g), due to the higher density of argon. In fact, the total pore volume calculated considering a fluid density of 1.4 cm^3/g, for argon, and 0.808 cm^3/g, for nitrogen, achieves a value of 1.32 cm^3/g for both adsorptives, in agreement with the Gurvitsch rule. The Gurvitsch rule states that the total amount adsorbed when expressed as a volume of liquid (assuming normal liquid density) at or near saturation vapour pressure is usually nearly the same for all adsorptives on a given adsorbent. Concerning the desorption branch, there is in both cases an important evaporation step, the lower closure point of the hysteresis loop being at a slightly lower relative pressure for argon compared to nitrogen.

Figure 3b shows the pore size distribution obtained from both isotherms after application of the non-local density functional theory (NLDFT equilibrium model) method and considering a cylindrical-shape pore model for the mesopores. The calculations were not extended to the microporous region. Concerning the mesoporous range, there are in both cases at least three contributions, two of them in the small mesopores region (around 2.1 and 3.5 nm) and a third large contribution at 4.7 nm for argon and 5.6 nm for nitrogen. As described above, the pore size analysis obtained from the nitrogen and argon data after application of a proper mathematical method for the calculation of the pore size distribution (PSD) is very useful to ascertain the evaporation mechanism. As it can be observed in Figure 3b, PSD calculated from the desorption branches for nitrogen and argon are drastically different, which confirms that the pore size is highly sensitive to the nature of the adsorbate molecule and not to the neck diameter. Consequently, *cavitation* is the dominant mechanism of the evaporation. In the case of cavitation, the desorption occurs at a relative pressure which is higher than the pressure of equilibrium evaporation from the pore neck and, consequently, no quantitative information about the neck diameter can be obtained (see inset in Figure 3a for a schematic representation of the mesoporous network). This

drawback has been overcome very recently by the development of a novel QSDFT method which takes into account the delay in condensation for nitrogen at 77.4 K [24]. Application of this novel approach to the nitrogen adsorption branch provides a more realistic picture, in a quantitative basis, of the mesoporous structure on samples where cavitation effects are observed. As it can be observed in Figure 3c, sample LMA22 exhibits an important contribution between 3-4 nm, which must correspond to the mesoporous necks, together with a second contribution above 20-30 nm, corresponding to the large mesocavities, in close agreement with TEM images.

At this point it must be highlighted that a similar mesoporosity development (not shown) in terms of pore volume and hysteresis phenomena has been observed for activated carbons prepared from other lignocellulosic precursors (olive stones) after application of the synthetic route described in this manuscript, i.e. a first chemical activation with $ZnCl_2$ followed by a subsequent physical activation with CO_2 and catalyzed with $CaCl_2$. Consequently, the described experimental procedure can be proposed as a good approach for the development of highly developed well-defined mesoporous activated carbons using natural products (lignocellulosic residues) as carbon precursors.

4. Conclusions

Mesoporous activated carbons have been successfully prepared from lignocellulosic precursors (peach and olive stones) using a combination of the traditional chemical and physical activation procedures. The synthesized activated carbons exhibit a well-developed micro and mesoporous structure with an "apparent" surface area around 1500 m^2/g and a mesopore volume up to 0.63 cm^3/g. Gas adsorption studies using nitrogen and argon at 77.4 K and 87.3 K, respectively, show that the mesoporous structure is mainly constituted of large mesoporous cavities (~20-30 nm) connected with the external surface through narrower mesoporous necks (~3-4 nm), i.e. cavitation effects are clearly observed.

Acknowledgment

Authors acknowledge financial support from a Strategic Japanese-Spanish Cooperative Program: Nanotechnologies and New Materials for Environmental Challenges (PLE2009-0052). Support from the EU (Contract FRESP ECGA nº 218138), MEC (projects MAT2007-61734 and PLE2009-0052) and Generalitat Valenciana (PROMETEO/2009/002) is also acknowledged.

References

[1] Marsh H, Rodriguez-Reinoso F, Activated Carbon. Elsevier: London; 2006.

[2] Yushin G, Hoffman EN, Barsoum MW, Gogotsi Y, Howell CA, Sandeman SR, et al. Mesoporous carbide-derived carbon with porosity tuned for efficient adsorption of cytokines. Biomaterials 2006;27:5755-62.

[3] Lei S, Miyamoto J-I, Kanoh H, Nakahigashi Y, Kaneko K. Enhancement of the methylene blue adsorption rate for ultramicroporous carbon fibers by the addition of mesopores. Carbon 2006;44:1884-90.

[4] Tao Y, Kanoh H, Abrams L, Kaneko K. Mesopore-modified zeolites: preparation, characterization, and applications. Chem. Rev. 2006;106:896-910.

[5] Yang H, Zhao D. Synthesis of replica mesostructures by the nanocasting strategy. J. Mater. Chem. 2005;15:1217-31.

[6] Ryoo R, Hoon Joo S, Jun S. Synthesis of highly ordered carbon molecular sieves via template-mediated structural transformation. J. Phys. Chem. B 1999;103(37):7743-6.

[7] Jun S, Hoon Joo S, Ryoo R, Kruk M, Jaroniec M, Liu Z, et al. Synthesis of new, nanoporous carbon with hexagonally ordered mesostructure. J. Am. Chem. Soc. 2000;122:10712-3.

[8] Gierszal KP, Jaroniec M. Carbons with extremely large volume of uniform mesopores synthesized by carbonization of phenolic resin film formed on colloidal silica template. J. Am. Chem. Soc. 2006;128:10026-7.

[9] Liang C, Dai S. Synthesis of mesoporous carbon materials via enhanced hydrogen-bonding interaction. J. Am. Chem. Soc. 2006;128:5316-7.

[10] Tanaka S, Nishiyama N, Egashira Y, Ueyama K. Synthesis of ordered mesoporous carbons with channel structure from an organic-organic nanocomposite. Chem. Commun. 2005:2125-7.

[11] Molina-Sabio M, Gonzalez MT, Rodríguez-Reinoso F, Sepúlveda-Escribano A. Effect of steam and carbon dioxide activation in the micropore size distribution of activated carbon. Carbon 1996;34(4):505-9.

[12] Molina-Sabio M, Rodriguez-Reinoso F. Role of chemical activation in the development of carbon porosity. Colloids and Surfaces A: Physicochem. & Eng. Aspects 2004;241:15-25.

[13] Juárez-Galán JM, Silvestre-Albero A, Silvestre-Albero J, Rodríguez-Reinoso F. Synthesis of activated carbon with highly developed "mesoporosity". Microp. Mesop. Mater. 2009;117:519-21.

[14] Hu Z, Srinivasan MP, Ni Y. Preparation of mesoporous high-surface-area activated carbon. Advanced Materials 2000;12(1):62-5.

[15] Silvestre-Albero J, Gómez de Salazar C, Sepúlveda-Escribano A, Rodríguez-Reinoso F. Characterization of microporous solids by immersion calorimetry. Colloids and Surfaces A: Physicochem. & Eng. Aspects 2001;187-188:151-65.

[16] Ravikovitch PI, Vishnyakov A, Russo R, Neimark AV. Unified approach to pore size characterization of microporous carbonaceous materials from N_2, Ar and CO_2 adsorption isotherms. Langmuir 2000;16:2311-20.

[17] Neimark AV, Lin Y, Ravikovitch PI, Thommes M. Quenched solid density functional theory and pore size analysis of micro-mesoporous carbons. Carbon 2009;47:1617-28.

[18] Almansa C, Molina-Sabio M, Rodriguez-Reinoso F. Adsorption of methane into $ZnCl_2$-activated carbon derived discs. Microp. Mesop. Mater. 2004;76:185-91.

[19] Silvestre-Albero A, Silvestre-Albero J, Sepúlveda-Escribano A, Rodriguez-Reinoso F. Ethanol removal using activated carbon: Effect of porous structure and surface chemistry. Microp. Mesop. Mater. 2009;120:62-8.

[20] Gregg SJ, Landford JF. Evaluation of microporosity, with special reference to a carbon black. Trans. Faraday Soc. 1969;65:1394-00.

[21] Rodríguez-Reinoso F, Garrido J, Martín-Martínez JM, Molina-Sabio M, Torregrosa R. The combined use of different approaches in the characterization of microporous carbons. Carbon 1989;27:23.

[22] Thommes M, Smarsly B, Groenewolt M, Ravikovitch PI, Neimark AV. Adsorption hysteresis of nitrogen and argon in pore networks and characterization of novel micro- and mesoporous silicas. Langmuir 2006;22:756-64.

[23] Rasmussen CJ, Vishnyakov A, Thommes M, Smarsly BM, Kleitz F, Neimark AV. Cavitation in metastable liquid nitrogen confined to nanoscale pores. Langmuir 2010;26(12):10147-57.

[24] Gor GY, Thommes M, Cychosz KA, Neimark AV. Quenched solid density functional theory method for characterization of mesoporous carbons. Carbon 2011 (submitted).